Article:
Khodaparast, S, Marcos, J, Sharratt, WN et al. (2 more authors) (2021) Surface-Induced Crystallization of Sodium Dodecyl Sulfate (SDS) Micellar Solutions in Confinement. Langmuir, 37 (1). acs.langmuir.0c02821. pp. 230-239. ISSN 0743-7463

https://doi.org/10.1021/acs.langmuir.0c02821

Surface-induced crystallisation of Sodium Dodecyl Sulfate (SDS) micellar solutions in confinement

Sepideh Khodaparast,*,† Julius Marcos,‡ William N. Sharratt,‡ Gunjan Tyagi,‡ and João T. Cabral‡

†*School of Mechanical Engineering, University of Leeds, LS2 9JT Leeds, UK*

‡*Chemical Engineering Department, Imperial College London, SW7 2AZ London, UK*

E-mail: s.khodaparast@leeds.ac.uk

Abstract

We investigate the role of confinement on the onset of crystallisation in sub-cooled micellar solutions of sodium dodecyl sulfate (SDS), examining the impact of sample volume, substrate surface energy, and surface roughness. Using small angle neutron scattering (SANS) and dynamic light scattering (DLS), we measure the crystallisation temperature upon cooling, and the metastable zone width (MSZW), for bulk 10-30 wt% SDS solutions. We then introduce a microdroplet approach to quantify the impact of surface free energy (18-65 mN/m) and substrate roughness ($R_\alpha \simeq$ 0-60 μm) on the kinetics of surface-induced crystallisation through measurements of induction time (t_i) under isothermal conditions. While t_i is found to decrease exponentially with decreasing temperature (increasing sub-cooling) for all tested surfaces, increasing surface energy could cause a significant, further reduction, of up to $\sim$40 fold. For substrates with the lowest surface energy and longest t_i, microscale surface roughness is found to enhance crystal nucleation, in particular for $R_\alpha \geq 10$ μm. Finally, we demonstrate that

tuning surface energy and microscopic roughness can be effective routes to promote or delay nucleation in bulk-like volumes, thus greatly impacting the stability of surfactant solutions at lower temperatures.

Introduction

Solution crystallisation underpins the manufacture of a wide range of materials, such as pharmaceutical drugs, food products and personal care formulations.[1–5] While the focus of some branches of pharmaceutical and food industries is on the promotion of crystal formation and control of their polymorphic structure, the inhibition of crystallisation can also be desirable in the production of soluble drugs and functional stable home care products. As the key component in personal and home care formulations, surfactants are amphiphilic molecules which can spontaneously self-assemble into ordered structures. At low to moderate concentrations (<30-40 wt%), most surfactants form globular micelles, extensively used in cleaning, foaming and encapsulation applications. Inevitable variations in temperature, and particularly cooling, can reduce the solubility of surfactants leading to the formation of crystals, hence compromising the long-term stability and overall performance of such micellar suspensions.[6–8] Cooling crystallisation is of special concern particularly for systems whose minimum solubility temperature is near room temperature (∼20 °C) for typical concentrations used in formulated products (5-30 wt%).[9] Well-known surfactants in this category include CetylTrimethylAmmonium Bromide (CTAB)[10] and Sodium Dodecyl Sulfate (SDS)[11] which are widely used in detergent formulations,[12] pharmaceutical products,[13–17] and bio-[18–22] and nano-technology[23–26] processes.

Crystallisation is a first-order phase transition initiated by nucleation events whose thermodynamics is often described in simple terms by the Classic Nucleation Theory (CNT).[27,28] CNT provides a minimal model for describing various scenarios of homogeneous nucleation in a supersaturated bulk solution. In practice, however, even at high level of supersaturation, bulk crystallisation occurs via a heterogeneous process initiated by nucleation on impurities

(indicated by case 1 in Fig. 1).[29–32] Additionally, solution crystallisation is often initiated in the vicinity of an interface with another material which may exist in either gas, liquid or solid phases or a combination of these, as illustrated schematically by cases 2-4 in Fig. 1.[33,34] Controlling heterogeneous crystallisation in the bulk is often challenging due to an incomplete knowledge of the structure, size and interfacial properties of impurities. By contrast, surface-induced crystallisation on solid confinement boundaries of prescribed characteristics offers robust routes to examine the role of the various physico-chemical variables.[35–41] Additionally, manifestations of confined and substrate-induced crystallisation are expected to be prevalent, and amplified, in common analytical laboratory processes, which employ smaller and geometrically confined sample volumes, such as those encountered in optical microscopy analyses, microfluidic platforms and differential scanning calorimetry (DSC).[42–44] Therefore, understanding the role of commonly-used laboratory substrates on heterogeneous phase change processes is crucial for the realistic interpretation of a range of experimental characterisation measurements.

Bulk crystallisation of SDS from aqueous solutions has been the topic of investigations for several decades.[45–48] Inevitably, most scientific characterisation procedures as well as practical applications that involve manipulation of SDS solutions undergo surface-induced crystallisation which precedes the nucleation within the bulk. In the last two decades, considerable research has been dedicated to analyses of surface-induced crystallisation of a variety of chemical compounds such as salts,[39,49] synthetic and natural polymers[41,50–52] and complex pharmaceutical formulations.[37,53] By contrast, heterogeneous crystallisation of surfactants has received comparably little attention in the literature and, to our knowledge, no systematic measurement of the impact of solid surfaces on cooling crystallisation of SDS or similar surfactant solutions has been reported. The main goal of this work is therefore to examine the role of confining solid boundaries, in particular the contribution of surface energy and microscopic surface roughness, on heterogeneous cooling crystallisation of SDS solutions.

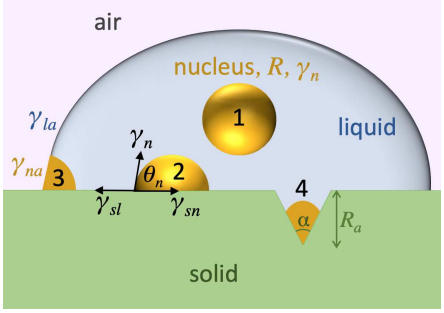

Figure 1: Schematic of different scenarios of bulk (1) and surface-induced (2, 3, and 4) nucleation considered in this study. R is the radius of the nucleus (in yellow) growing within the sub-cooled liquid phase (in blue). γ_n is the average interfacial energy between the nucleus and the bulk, and θ_n is the contact angle of the nucleus on the solid substrate. γ_{sl}, γ_{ns} and γ_{la} are solid-liquid, solid-nucleus and liquid-air (surface tension of the liquid) interfacial energies. α is the roughness wedge angle and R_a refers to the average surface roughness.

We first examine the bulk crystallisation in micellar solutions of SDS in the range of 10-30 wt% in cooling experiments using Small Angle Neutron Scattering (SANS) and Dynamic Light Scattering (DLS), in conditions of negligible impact from the solid boundaries. We measure the solubility boundary of SDS solutions of prescribed concentrations upon cooling and identify the corresponding metastable region in the temperature-concentration phase diagram. Secondly, we focus on surface-induced heterogeneous crystallisation and investigate the effect of free surface energy and roughness of the substrates in contact with μL volumes of micellar solutions of SDS in confined geometry, where interfacial effects are significant. Finally, we validate our findings of surface-induced heterogeneous crystallisation gathered from confined micro-scale geometries in large 'bulk' sample volumes.

Experimental

Sodium dodecyl sulfate SDS (>99.0% purity) was purchased from Sigma-Aldrich and used as received. Solutions for DLS and OM measurements were prepared by diluting SDS in deionised water and keeping the solutions at room temperature overnight. Surfactant solutions were filtered (0.2 μm PTFE syringe filter) before use. For SANS measurements, SDS at >99.0% purity was diluted in D_2O. Considering the density difference between H_2O and

D_2O, a correction was made when preparing samples in D_2O to keep the molar fraction of surfactant constant.

Dynamic Light Scattering (DLS)

Dynamic light scattering (DLS) was performed using a Zetasizer Nano S (Malvern Panalytical), which operates in back-scattering ($\theta = 173°$) with a 633 nm He-Ne laser yielding $q = 0.0026$ Å^{-1}. The cuvette temperature was controlled with a Peltier system in the range of 30 °C to 0 °C. All cooling cycles were started from 30 °C to ensure that samples were initially in the isotropic micellar phase, samples were left to reach thermal equilibrium at the final temperature T_f and time-resolved data were acquired over one hour to probe the transition from micellar to crystalline phases. To achieve the largest $\Delta T/\Delta t$ in isothermal DLS experiments, the test environment was stabilised at T_f before inserting the cuvette containing the sample. Data were acquired in triplicate. The raw correlograms were interpreted without any need for cumulant fitting or CONTIN analysis, in order to identify the boundaries of the micellar phase.

Cross-polarised Optical Microscopy (OM)

Cross-polarised optical microscopy was used to detect phase transition from the isotropic micellar phase to the birefringent crystalline phases, following procedures described in a previous publication.[7] Approximately 0.5 μl of the solution was placed between two thin glass cover slips. Solvent evaporation during the experiments was minimised by sealing the area surrounding the droplet using an adhesive gasket of 120 μm thickness. Solvent evaporation was further controlled during the image processing step by ensuring that the droplet area remained constant during the experiments. Any measurement showing droplet shrinkage was discarded from the data set. Isothermal experiments were performed by initially stabilising the droplet at 30 °C before a rapid quench (at 80 °C/min) to the final temperature of interest. Thermal control of the microscopic samples was carried out using a Linkam THMS600

temperature control stage. OM images were captured with an Olympus BX41M-LED microscope, using 5X and 10X objectives and a CMOS camera (Basler ac2040-90).

Small Angle Neutron Scattering (SANS)

SANS experiments in linear and isothermal cooling cycles were performed on the Larmor diffractometer (ISIS, Harwell, UK), with a polychromatic λ=0.9-13.3 Å incident beam and sample-to-detector distance = 4.1 m, yielding a fixed momentum transfer range of approximately $0.005 < Q < 0.6$ Å^{-1} with the peak flux in the intermediate Q range. Quartz cells (1 mm banjo pathlength, Starna) containing micellar solutions of SDS were installed into a metallic sample changer that was thermally controlled using a liquid bath. Experiments were started at 60 °C, where all solutions were in the isotropic micellar phase, and then a variety of cooling ramps were applied to the samples to reach 0 °C.[7] The resulting SANS data were reduced, using standard procedures, in MANTID.[54]

Profilometry and surface roughness

Polydimethylsiloxane (PDMS) surfaces of prescribed roughness were prepared by pouring 10:1 (base:cross-linker) solution of Sylgard 184 (Dow Corning) over sandpaper of different roughness, degassed under a vacuum desiccator and baked at 80 °C overnight. Patterned PDMS slabs were then peeled off and used as rough substrates. High fidelity replication of three-dimensional micro- and nano-structure of sandpaper by using PDMS was previously reported in the literature.[55] A Bruker DektakXT stylus profiler was used to quantify the surface roughness of various PDMS slabs. Stylus force was set at 2 mg and a map of 2 μm resolution over an area of 4 $\times$ 4 mm^2 was obtained for each sample. The arithmetical mean deviation of the measured profile R_a was used as an estimate of the surface roughness (detailed in SI).

Surface plasma treatment and contact angle

A series of glass (Fisherbrand borosilicate glass coverslips), polycarbonate (Goodfellow, 325-170-20) and PDMS (1:10, Sylgard 184) substrates were investigated. A Harrick PDC 13.6 MHz oxygen plasma cleaner was employed to tune surface free energy. A power of 18 W and exposure times of 2 min were used, and the resulting contact angles were measured with a digital camera setup.

Results and discussion

Due to its wide range of applications, the phase behaviour of aqueous solutions of SDS and its hydrated crystals, at equilibrium and in static conditions, have been extensively investigated over the past decades.[11,46,56–59] Nevertheless, the kinetics of phase transformations upon variations of temperature and concentration, and those occurring in the vicinity of interfaces remain largely unresolved. Here, we focus on transformations from the micellar L_1 to the crystalline C phase that occur upon cooling at fixed surfactant concentration. We first describe signatures of the two phases obtained through conventional analytical methods focusing on nucleation of SDS crystals within the bulk solution. Next, we investigate the impact of solid boundaries, particularly surface energy and roughness on heterogeneous nucleation of SDS within micellar solutions in confined settings.

Bulk crystallisation

Above the Critical Micelle Concentration (CMC) at about 8.2 mM[60] and below 30-40 wt% of surfactant, aqueous solutions of SDS exist in micellar L_1 phase at temperatures above 25 °C. In this temperature-concentration range, ellipsoidal micelles of SDS elongate and become less negatively charged with decreasing temperature.[61,62] Upon continuous cooling below room temperature, hydrated crystalline SDS structures (C) are formed within the micellar solutions (L_1).[62] We employed DLS to monitor the formation of crystals in the solution with

nanoscale resolution in mL volumes of 10-30 wt% SDS. In all experiments, very slow cooling ramps (ΔT/Δt $<$ 0.5 °C/min) combined with temperature steps of $\Delta T = 1$ °C and 30 min waiting time at each step is applied to ensure sample thermal equilibrium (Fig. 2a). Without further analysing the correlograms obtained from DLS analyses, nucleation and growth of the crystal within the micellar solutions of SDS can be simply detected by tracking the appearance of a time-dependent slow-decay mode at lower temperatures (Fig. 2b). At 20 wt% SDS, no crystalline phase exists at room temperature, while a clear phase transformation was detected at about 13 °C. In parallel, SANS measurements detected formation of larger hydrated SDS crystals at temperatures below 14 °C for 20 wt% SDS, manifested by an upturn in lower-Q region alongside a clear sharp Bragg peak at higher Q, characteristic of the lamellar crystalline strcuture (Fig. 2c). The Bragg diffraction peaks at 0.192 Å^{-1} (lamellar spacing, $d = 32.7$ Å) and 0.378 Å^{-1} respectively correspond to the first and second lamellar spacing of the SDS-rich crystalline structure.[44,46] The crystalline lamellar structures are birefringent and clearly observed using cross-polarised optical microscopy OM (Fig. 2d).

At a fixed concentration of SDS, the temperature that the crystallisation is first detected upon cooling $T_{C,C}$ is much lower than the equilibrium solubility temperature $T_{C,H}$ since a sufficient level of sub-cooling is required to induce spontaneous nucleation in the solution. The extent of sub-cooling temperature required to obtain crystallisation at a given concentration is identified as the MetaStable Zone Width (MSZW), see Fig. 2d.[48,63,64] The MSZW is a strong function of the rate of cooling applied, purity and volume of the sample, and the detection resolution of the experimental technique used in continuous cooling experiments. In practice, most of these variables cannot be independently controlled since the experimental measurement approach dictates not only the spatial detection resolution, but also the sample volume which in turn impacts the cooling rate, *i.e.* the larger the sample volume the slower the cooling rate that the bulk solution experiences. Moreover, besides the geometry, the experimental approach often limits the choice of sample container material which can significantly affect the observed crystallisation temperature by promoting surface-

induced heterogeneous crystallisation, especially as the surface-to-volume ratio of the sample increases. Therefore, any interpretation and comparison of the MSZW measurement reports must carefully consider the experimental technique and protocols in use.

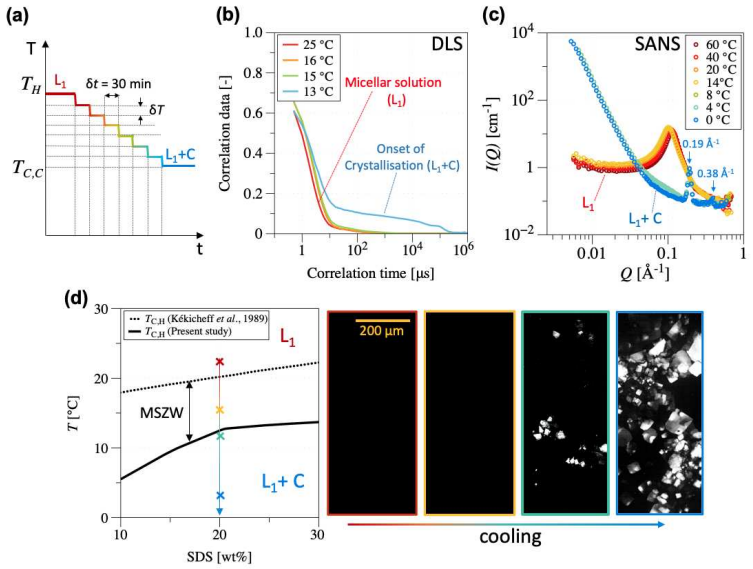

Figure 2: Detection of crystallisation in aqueous micellar solution of SDS upon continuous, stepped, slow cooling. (a) Schematic example of a cooling path starting from T_H in L_1 phase until reaching $T_{C,C}$ in L+C phase. (b) DLS measurements show the appearance of fast-growing larger objects with long decay times, in addition to the primary micellar aggregates, as the 20 wt% SDS solution is cooled below $T = 15$°C. (c) Upon cooling of the SDS solutions below $T < 14$°C, the micellar peak in SANS measurements at intermediate-Q gradually disappears as a Bragg peak at high-Q and upturn at low-Q, both associated with the crystallisation of SDS, are detected. The diffraction Bragg peaks at 0.192 Å^{-1} and 0.378 Å^{-1} respectively correspond to the first and second lamellar spacing of SDS-rich crystalline structure. (d) Upon cooling the micellar phase, crystallisation occurs at $T_{C,C}$ (solid line) that is lower than the temperature at which the crystals disappear $T_{C,H}$ (dotted line[11,57]) in a reverse heating cycle. The L_1 and L_1+C phases are separated by a metastable zone. Cross-polarised optical microscopy images of solutions of 20 wt% SDS show growth of crystals as the solution is cooled below 13°C. The isotropic micellar phase (L_1) appears black, while the crystalline phase C is birefringent.

Owing to the relatively large sample volume and high detection resolution, SANS and DLS measurements allow precise tracking of static nucleation and crystallisation in the bulk based on the assumption of negligible contribution from sample interaction with its surrounding solid boundaries. However, rational comparison of kinetic measurements obtained from different analytical tools, where significant contribution of non-homogeneous nucle-

ation is likely, largely relies on mechanistic understanding of surface-induced heterogeneous nucleation. In the following sections, we use DLS as a facile tool to characterise the bulk crystallisation of SDS solutions at a given concentration (20 wt%) and compare results with those obtained by optical microscopy analyses of microdroplets in order to assess the potential impact of interactions with typical bounding interfaces.

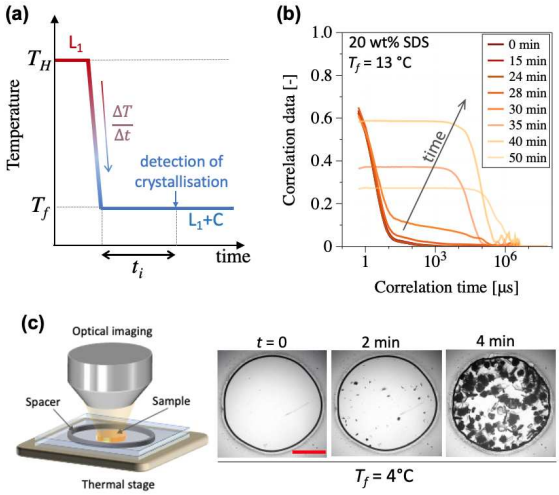

Figure 3: Induction time of crystallisation in isothermal DLS experiments for SDS solutions. (a) Schematic of a typical thermal path followed in isothermal DLS and OM tests. The induction time t_i is measured from the initial time that sample is exposed to T_f. (b) The nucleation and growth of crystals are identified through the appearance a slow-mode decay in the raw DLS correlograms, here after 28 min at 13 °C. (c) Microdroplet experiment: a droplet of 20 wt% SDS solution is confined between two identical transparent substrates that are sealed around the droplet to minimise the evaporation. The sample is placed on top of a thermally controlled stage and is subsequently quenched at 80 °C/min to reach the final temperature T_f. Micro-graphs correspond to OM images of a confined droplet at 4 °C (here using glass substrates), in which crystallisation occurs within the first minute of reaching T_f. Scale bar corresponds to 500 μm.

Isothermal measurements and induction time

In order to eliminate the effect of cooling rate as a variable in our measurements, here we perform isothermal tests in which the micellar solution is rapidly cooled to the final temperature T_f and held isothermally for 60 min during which continuous time-resolved detection of any possible crystallisation in the solution is performed (Fig. 3a). Under isothermal conditions,

the time required for the critical nucleus formation and growth of a detectable crystalline phase in a supersaturated solution is referred to as the induction time t_i.[65] Induction time provides a convenient measure of the supersaturation level within the solution, while providing an indirect tool for estimating kinetics of nucleation and crystal growth.[37,65,66]

Miller *et al.* (2016) measured the induction time for SDS solutions in isothermal tests, however, their measurement showed no crystal formation for $T_f > 5$ °C at 20 wt%, and yielded a wide metastable zone considering the corresponding equilibrium solubility temperature of 20 °C.[47] Note that the induction time here refers to the time required for the formation of detectable crystalline phase from an equilibrium micellar phase. Using Differential Scanning Calorimetry (DSC), Summerton *et al.* (2016) observed crystallisation at around 12±1°C for 20 wt% SDS solutions, which is closer to the equilibrium phase transition, but no information on the kinetics of crystallisation and induction time was provided.[44] In our isothermal DLS tests, no detectable change was found within 60 min of reaching $T_f > 14$ °C in micellar solution of 20 wt% SDS. A clear change in the correlation data attributed to the emergence of crystals was found only after 25 min at $T_f = 13$ °C (Fig. 3b). This finding emphasises the sensitivity of MSZW measurements of similar systems to the experimental protocol followed even under identical isothermal test conditions. Given that the induction time is expected to be extremely large near the phase boundary, it is practically difficult to measure accurately and often may be missed if samples are not equilibrated for long enough. In general, in the range of 10-30 wt% of SDS, the cooling crystallisation temperatures detected here by DLS matched those reported previously based on DSC measurements (Fig. SI1).[44]

Surface-induced crystallisation

While isothermal experiments effectively determine the impact of sub-cooling on the induction time of crystallisation, other conditions can dramatically influence the induction time of crystallisation. Such conditions are often achieved by promoting heterogeneous crystalli-

sation of the solution on additional surfaces and boundaries.[37,67,68] Here, we characterise the effect of surface energy and topography of solid interfaces on the crystallisation induction time of micellar solutions of SDS through OM analyses of confined microdroplets, where the contribution of the surface effects is maximised. Fig. 3c shows a schematic of the microdroplet experimental setup used in this study. An isothermal quenching test similar to that represented in Fig. 3a is applied to the bottom substrate (here glass) on which the microdroplet of solution of 20 wt% SDS rests. It is practically simpler to impose a well-controlled cooling ramp in the microdroplet experimental setting thanks to the small volume of the sample, large surface area in contact with the cooling device and precise control of thermal ramps imposed by the thermal stage. All isothermal cooling crystallisation tests reported here are thus achieved by initial cooling of the micellar droplet at 80 °C/min. The microdroplet setup allows microscopic detection of various hydration states of SDS in the crystals, which are correlated to their morphology,[47] and their growth in time thanks to the relatively high temporal resolution of the optical imaging apparatus (here on the order of 10^{-2} s) and fast thermal equilibrium of the sample.[48]

As expected, the induction times t_i measured by DLS and OM significantly decrease upon decreasing the final temperature T_f and reaching higher sub-cooling ΔT in solution (Fig. 4). Considering that the volume of the sample and the detection length-scales have been simultaneously reduced by $\sim$3 orders of magnitude in microdroplet experiments compared to DLS, the induction time for detection of bulk crystallisation in the microdroplet setup could be expected to be significantly longer. Note that effects of confinement due to the higher level of supersaturation in the nano-litre environment is negligible here.[69] However, comparison between microdroplet and DLS measurements at similar conditions presented in Fig. 4 shows a significant reduction in t_i for OM analyses performed on smaller sample volumes. This observation indicates that the crystallisation observed in microdroplets is promoted by the considerably larger contact area of the sample with the bounding surfaces, and thus larger surface-area to volume ratio, $SA : V$, as shown in Fig. 4 (see SI for more

details). Next, we explore the impact of free energy and microscopic roughness of the surface on the SDS crystal nucleation in microdroplet experiments through measurement of t_i.

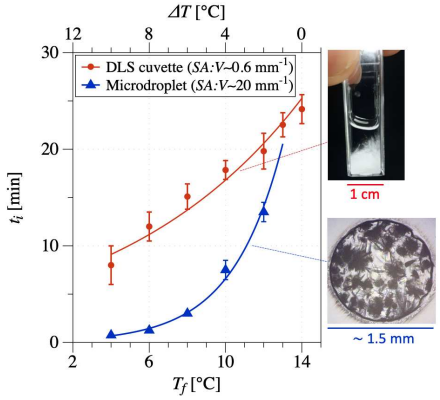

Figure 4: Comparison between induction time measurements using DLS for 1 mL of solution and microscopy (on glass substrates) for a droplet of ≈ 0.5 μL volume. Solutions contain 20 wt% of SDS. The induction time decreases with reducing the final sub-cooled temperature T_f. Due to the large volume of the samples requiring relatively long thermal equilibrium time and low temporal resolution of DLS, shorter induction times expected at $T_f < 4$ °C are not considered here. ΔT corresponds to $T_{C,C} - T_f$ and Surface-area to volume ratio $SA : V$ is calculated considering all air-liquid interfaces and solid surfaces. Images on the right show examples of SDS crystallisation in aqueous micellar solution in a DLS cuvette (top) and microscopic droplet (bottom).

Surface free energy

We investigate the impact of surface energy for substrates that are relevant to laboratory-scale crystallisation measurements (e.g., in sample vials, or microfluidic devices), namely glass, PDMS and polycarbonate (PC). To modify the surface energy of the glass, used in measurements presented in Fig. 3, we use an oxygen plasma treatment. Plasma treatment is a common processing step, used in industrial and laboratory environments, to increase the surface free energy, and enhance molecular interactions and adhesion on the surface,[75,76] as well as in the surface bonding and sealing of micro-devices.

Our microdroplet experiments on plasma-treated glass show significantly faster induction of crystal nucleation and larger number density of crystals compared to those on untreated glass, as shown in the image sequences in Fig. 5a. At a given temperature (here $T_f = 12$ °C)

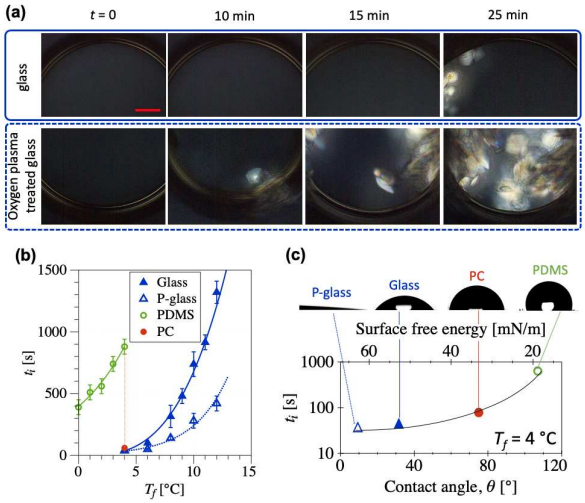

Figure 5: Effect of surface energy on surface-induced isothermal crystallisation of 20 wt% micellar SDS solutions. (a) Cross-polarised OM time lapse images of microdroplets sandwiched between glass cover-slips without (top) and with (bottom) oxygen plasma treatment (for 2 min) at $T_f = 12$ °C. On the native glass substrate, no crystals are formed within the first 20 min of reaching T_f. Plasma treatment of the glass substrate significantly promoted crystal nucleation and detectable crystals were observed within 10 min of reaching the final temperature. The scale bar corresponds to 300 μm. (b) Induction times t_i measured on glass, oxygen plasma treated glass (P-glass), PDMS and polycarbonate substrates as a function of T_f. The dashed line represent the condition at which measurements in panel (c) are collected. (c) Induction time t_i measurements vs contact angle of water on different surfaces at $T_f = 4$ °C. Average surface free energy values reported in the literature are provided as a reference.[70–74] Images show wetting conditions for DI water droplets on the different tested substrates.

no SDS crystals were detected on the surface of untreated glass in the first 20 min, while clear birefringent crystalline structures were visible on plasma-treated glass within 10 min of reaching T_f. Plasma oxidation significantly increases the free surface energy of glass (from $\simeq$60$\pm$7 mN/m to 70$\pm$7 mN/m), rendering it more hydrophilic. In order to further verify our conclusion that heterogeneous crystallisation of SDS is enhanced by increasing total surface free energy, we measure the crystallisation t_i for 20 wt% micellar solutions for a range of final temperatures 4 °C $< T_f <$ 12 °C on glass, plasma-treated glass (P-glass), and PDMS, see Fig. 5b. For all three surfaces, t_i decreases exponentially with decreasing T_f (Fig. 5b) and becomes closer to the lower boundary metastable zone (Fig. 2d). Considering the anionic nature of SDS, it is expected that the polar contribution of the surface free energy will

define the rate of interaction with the surfactant molecules and influence induction time of crystallisation, see Fig. SI3. Therefore, simple water contact angle measurements can adequately describe the impact of surface energy on SDS crystallisation as confirmed in Fig. 5c. For a given final temperature (here 4 °C), we found t_i to increase from ∼35 s on plasma-treated glass (contact angle ≈ 8°) to ∼80 s on polycarbonate PC (contact angle ≈ 75°) and finally to ∼650 s on PDMS (contact angle ≈ 107°). The corresponding total surface free energy values reported in the literature are included Fig. 5c as a reference, see Fig. SI3 for comparison between impacts of polar and non-polar surface energy contributions.[75–81]

The effect of the substrate free energy on t_i can be rationalised in terms of a lower contact angle of the heterogeneous SDS crystal nuclei forming on the solid substrate (θ_n in Fig. 1) of higher surface energy which in turn yields a lower nucleation energy barrier.[33] We note that crystallisation of aqueous micellar solutions of SDS is mainly controlled by the contribution of polar surface energy (Fig. SI3), which is clearly reflected in the contact angle of water droplets on the surface, see Fig. 5c. The interfacial energy between the substrate and crystalline phase depends on the absorption and adhesion of the solute molecules on the bounding solid surfaces which is generally governed by the attractive forces arising from chemical bonds, hydrogen bonds and van der Waals interactions,[82] whose cumulative contribution is quantified by the surface free energy.[83–85] Therefore, correlating t_i with surface free energy appears to provide a simple, practical approach to estimate the substrate impact on heterogeneous nucleation in surfactant crystallisation. More precise identification of molecular aspects of surface-induced crystallisation requires application of time-resolved experimental structural measurements and non-classical two-step theoretical analysis in the vicinity of the interface.[86–88]

Microscopic surface roughness

Another route for reducing the energy barrier to heterogeneous nucleation on substrates of low free energy is the introduction of roughness on the surface.[52,89] Roughness can be

modelled in terms of geometrical wedges of depth R_a constructed of smooth flat surfaces joined at an angle α, see case 4 in Fig. 1. Heterogeneous crystallisation becomes thus controlled not only by the interfacial energy and contact angle of the nucleus on the surface θ_n, but also by the wedge geometry, namely its depth and angle of the opening.[90–93] For wedges filled with the liquid phase, which are significantly larger than radius of a critical nuclei R, the energy barrier in CNT disappears when $\theta_n \ll 180° - \alpha$, *i. e.* deep narrow wedge geometries promote spontaneous nucleation.[34,91]

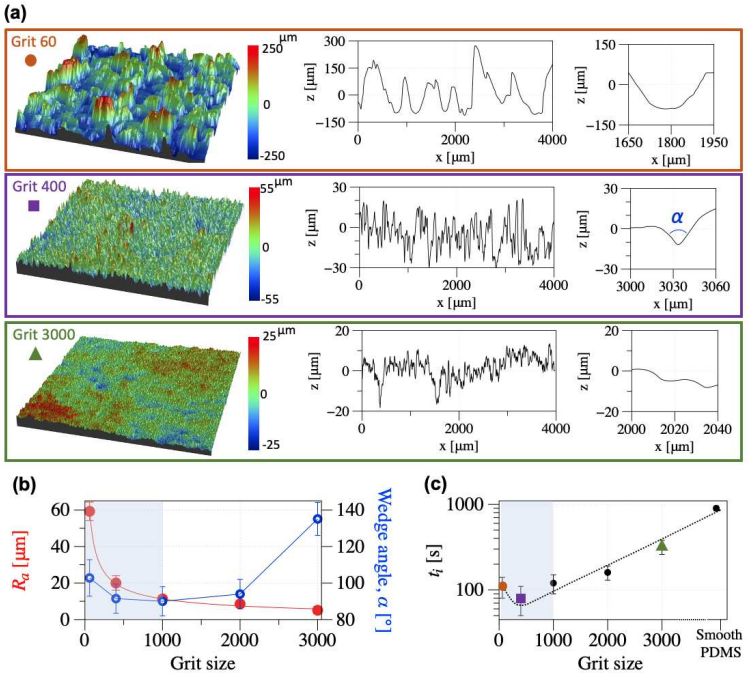

Figure 6: Promoting surface-induced heterogeneous crystallisation of SDS on PDMS substrates by introducing microscopic surface roughness. (a) Rough PDMS surfaces are fabricated using commercially available sandpaper at different grit numbers. Profilometry measurements on a 4 × 4 mm^2 are used to correlate the grit size with the quantitative surface roughness amplitude and shape. (b) Surface roughness R_a increases from about 5 μm for grit size 3000 to around 60 μm for grit size 60. The wedge angle α is estimated as the average of 10 different measurements performed across the rough PDMS substrates. Examples of typical wedges at different grit numbers are presented with scale bars representing 20 μm. Optimal rough surfaces for promoting faster heterogeneous nucleation are expected to exhibit larger amplitude of roughness while maintaining wedges of smaller internal angle, α, as highlighted by the blue strip. (c) The induction time is significantly reduced on rough PDMS substrates, especially as roughness in increased to 10 μm and above, corresponding to sandpaper grit number 1000 and smaller.

While most computational and experimental investigations of heterogeneous nucleation on rough surfaces have been dedicated to understanding the effect of nano-scale surface structures,[35,52,53,89,92,94,95] our goal here is to identify the impact of larger microscopic surface roughness,[96,97] where the wedge dimension is significantly larger than critical radius of the nucleus. To this end, we perform microdroplet experiments on rough PDMS substrates fabricated via a templating approach, using commercially available sandpaper of different grades. Thanks to its high efficacy in replicating surface structures down to sub-micron feature sizes and its low surface energy, PDMS offers a suitable substrate for quantifying the effect of surface roughness on heterogeneous surface-induced crystallisation without modifying surface chemistry.

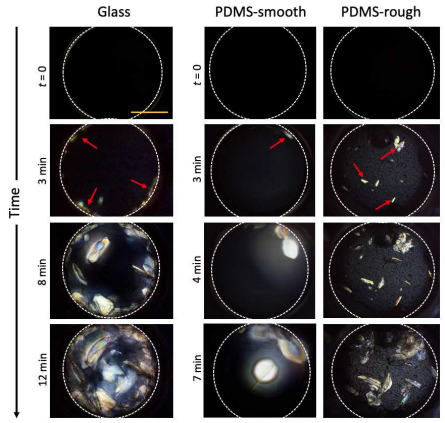

Figure 7: Time sequence of crystallisation in microdroplets on smooth glass, PDMS and rough PDMS (grit 2000) substrates, at T_f=3.5±0.5 °C. Crystal formation is initiated at the air-liquid interface around the droplets on smooth surfaces, in contrast to those appearing at the roughness sites on rough PDMS substrates. Scale bar refers to 500 μm.

Roughness of sandpaper is commonly quantified by the 'grit size', which refers to the size of the abrasive particles on its surface, and can thus be correlated with the amplitude of surface roughness. Fig. 6a shows surface topography of the PDMS substrates obtained using different grits of sandpaper as templates. A wide range of surface undulations with amplitudes ranging from around 100 μm down to about 5 μm were obtained using sandpapers with grit numbers ranging from 60 to 3000, respectively. We characterised the topography of the roughness by measuring both amplitude (R_a) and opening angle of the surface un-

dulation (α) by profilometry, Fig. 6b. Further information on surface roughness analyses is provided in SI. Computational molecular dynamic analyses at the nanoscale[32,33,93] predict that surfaces of larger roughness with deep narrow wedges offer ideal geometrical settings to promote surface-induced crystallisation. By analogy to our microscale roughness, this range corresponds to PDMS surfaces templated with grit sizes smaller than 1000 (shown in Fig. 6b), where roughness is found to significantly reduce t_i (Fig. 6c). In general, t_i measurements on PDMS surfaces of various roughness show that adding microscopic roughness to the PDMS surface dramatically reduces the crystallisation induction time (Fig. 6c). Relative to smooth PDMS substrates (towards the right end of the x-axis in Fig. 6c), more than an order of magnitude reduction in t_i is achieved by inducing wedges of depth larger 10 μm. A boomerang shaped curve with a minimum around grit size 400 describes the trend of t_i vs. surface roughness, similar to the results presented previously in the literature for nucleation from vapour on microscopically rough glass surfaces.[96] This observation confirms that effective promotion/inhibition of surface-induced crystallisation can be achieved by careful design of the roughness size and geometry.

We note that in the microdroplet experiments on smooth substrates, the initial primary crystallisation sites are typically located at the triple contact line between the liquid droplet, surrounding air and top/bottom solid substrates (first and second columns in Fig. 7). This observation is rationally supported by previous computer simulations by Sear[33] demonstrating that the rate of the nucleation is significantly larger at the three-phase contact point of air-water-solid impurities. The nucleation energy barrier at the air-liquid-solid interface (case 3 in Fig. 1) is significantly reduced by the lower contribution of the interfacial tension of nucleus due to the partial interface with the bulk liquid, which minimises the contribution of γ_n. Additionally, nucleation at the triple contact point substitutes the existing interfacial energies γ_{sl} and γ_{la} by the newly generated γ_{sn} and γ_{na}, respectively. Therefore, crystal nucleation is enhanced at the solid-liquid-air contact point on flat substrates, unless nucleation interfacial energies with the solid γ_{sn} and the gas phase γ_{na} are considerably large. Inter-

estingly, adding surface roughness not only accelerates the surface crystallisation on PDMS, but also clearly promotes nucleation and crystallisation within the droplet and not on the boundaries at the surrounding air interface, as was observed for flat smooth surfaces and highlighted by comparison of the third with the first two columns in Fig. 7.[33]

Conclusion

We have investigated the heterogeneous crystallisation of aqueous micellar solutions of SDS upon cooling. Using DLS and SANS we have characterised the 'bulk' metastable zone width MSZW. Comparison with previous reports[44,47] shows that the detection resolution of the experimental techniques in use, volume of the sample, and cooling rates imposed may significantly impact measurements of the MSZW. We introduced confined microdroplet cooling crystallisation experiments which amplify surface-induced crystallisation, and enable the examination of the effects of surface free energy and roughness on heterogeneous crystallisation through measurement on induction time, t_i. In general, heterogeneous nucleation in microdroplets was enhanced by increasing the surface free energy of the substrate and introducing microscopic roughness on the surface. Shortest crystallisation t_i was achieved on surfaces of large roughness amplitude and small roughness wedge angle.

As the sample surface-to-volume ratio decreases, one trivially expects the surface-induced heterogeneous nucleation to become less significant compared to the bulk nucleation, especially for smooth surfaces of low free energy. As confirmation, our experiments performed in clean untreated glass vials containing approximately 3 mL of 20 wt% SDS solutions show minimal crystallisation within 30 min of reaching the highest level supersaturation tested here at $T_f = 4$ °C, see images of the vials in top row of Fig. 8 for glass and smooth PDMS. For comparison, confined microdroplet experiments on smooth glass and PDMS crystallised within 1 and 16 min, respectively. Nevertheless, we predict that substrates with high free energy and/or microscopic roughness can play significant roles in promoting heterogeneous

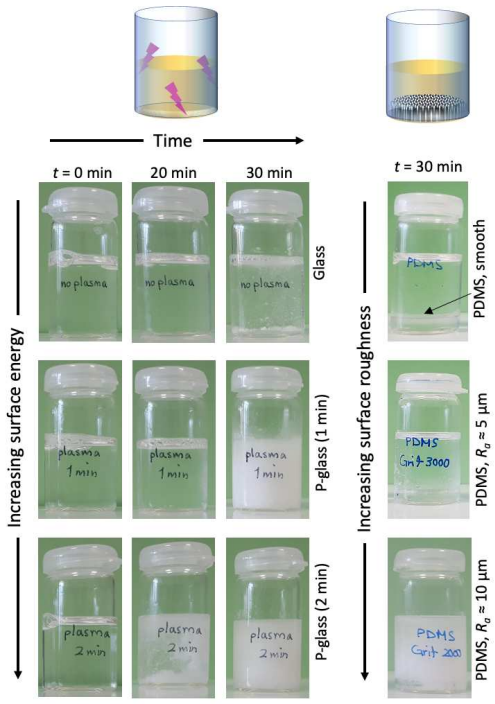

Figure 8: Crystallisation in glass vials containing ∼3 mL (bulk-like volume) of 20 wt% SDS solution at $T_f = 4$ °C over 30 min. Samples were cooled from 30 °C, at which SDS solutions are in the micellar L_1 phase. Plasma treatment of the internal surface of the glass vial accelerates the formation of SDS crystals. Exposure to 2 min oxygen plasma significantly reduces the nucleation induction time t_i compared to those exposed to 1 min plasma. Untreated glass vials show minimal crystallisation within 30 min of the test. Placing slabs of PDMS of increasing roughness on the bottom of the containers enhances the heterogeneous nucleation and increases the density of crystallisation relative to vials with no/smooth PDMS. The base diameter of the vials is 20 mm.

nucleation in larger volumes, and are thus important in practical applications. Fig. 8 confirms and quantifies the accelerated surface-induced crystallisation promoted by plasma treatment of the solid boundaries of the container, or by the introduction of rough surfaces. Evidently, understanding the impact of surfaces on heterogeneous crystallisation can be used to control the nucleation density and induction time via tuning the surface energy and roughness, even in 'bulk' volumes. The confined microdroplet approach employed here provides a facile yet rigorous tool to examine surface effects on heterogeneous crystallisation which can then be extended to larger volumes often encountered in material processing units, as well as in laboratory analyses.

Acknowledgement

We thank the National Formulation Centre (NFC) of the Centre for Process Innovation (CPI, UK), Procter & Gamble and BP-Castrol for funding the microSTAR partnership. Experiments at the ISIS Neutron and Muon Source were supported by a beamtime allocation RB1820374[98] from the Science and Technology Facilities Council. JTC acknowledges the Royal Academy of Engineering (UK) for funding a Research chair.

Supporting Information Available

The following files are available free of charge.

- Filename: SI for Surface-induced crystallisation of SDS micellar solutions in confinement (PDF)

References

(1) Chen, J.; Sarma, B.; Evans, J. M. B.; Myerson, A. S. Pharmaceutical Crystallization. *Crystal Growth & Design* **2011**, *11*, 887–895.

(2) Shekunov, B. Y.; York, P. Crystallization processes in pharmaceutical technology and drug delivery design. *Journal of Crystal Growth* **2000**, *211*, 122–136.

(3) Hartel, R. W. Advances in Food Crystallization. *Annual Review of Food Science and Technology* **2013**, *4*, 277–292.

(4) Ribeiro, A. P. B.; Masuchi, M. H.; Miyasaki, E. K.; Domingues, M. A. F.; Stroppa, V. L. Z.; de Oliveira, G. M.; Kieckbusch, T. G. Crystallization modifiers in lipid systems. *J Food Sci Technol* **2015**, *52*, 3925–3946.

(5) Hondoh, H.; Ueno, S.; Sato, K. *Fundamental Aspects of Crystallization of Lipids*; John Wiley Sons, Ltd, 2018; Chapter 4.

(6) Laughlin, R. G. *The aqueous phase behavior of surfactants*; Academic Press, 1996.

(7) Khodaparast, S.; Sharratt, W.; Wang, H.; Robles, E. S.; Dalgliesh, R.; Cabral, J. T. Spontaneous formation of multilamellar vesicles from aqueous micellar solutions of sodium linear alkylbenzene sulfonate (NaLAS). *Journal of Colloid and Interface Science* **2019**, *546*, 221 – 230.

(8) Summerton, E.; Hollamby, M. J.; Zimbitas, G.; Snow, T.; Smith, A. J.; Sommertune, J.; Bettiol, J.; Jones, C.; Britton, M. M.; Bakalis, S. The impact of N,N-dimethyldodecylamine N-oxide (DDAO) concentration on the crystallisation of sodium dodecyl sulfate (SDS) systems and the resulting changes to crystal structure, shape and the kinetics of crystal growth. *J. Colloid Interf. Sci.* **2018**, *527*, 260–266.

(9) Tadros, T., Ed. *Encyclopedia of Colloid and Interface Science*; Springer-Verlag Berlin Heidelberg, 2013.

(10) Amos, K. E.; Brooks, N. J.; King, N. C.; Xie, S.; Canales-Vázquez, J.; Danks, M. J.; Jervis, H. B.; Zhou, W.; Seddon, J. M.; Bruce, D. W. A systematic study of the

formation of mesostructured silica using surfactant ruthenium complexes in high- and low-concentration regimes. *J. Mater. Chem.* **2008**, *18*, 5282–5292.

(11) Kékicheff, P. Phase diagram of sodium dodecyl sulfate-water system: 2. Complementary isoplethal and isothermal phase studies. *Journal of Colloid and Interface Science* **1989**, *131*, 133–152.

(12) Johansson I., S. P. *Handbook for cleaning/decontamination of surfaces*; Elsevier, 2007.

(13) Balakrishnan, A.; Rege, B. D.; Amidon, G. L.; Polli, J. E. Surfactant-mediated dissolution: Contributions of solubility enhancement and relatively low micelle diffusivity. *Journal of Pharmaceutical Sciences* **2004**, *93*, 2064–2075.

(14) Ito, E.; Yip, K. W.; Katz, D.; Fonseca, S. B.; Hedley, D. W.; Chow, S.; Xu, G. W.; Wood, T. E.; Bastianutto, C.; Schimmer, A. D.; Kelley, S. O.; Liu, F.-F. Potential Use of Cetrimonium Bromide as an Apoptosis-Promoting Anticancer Agent for Head and Neck Cancer. *Molecular Pharmacology* **2009**, *76*, 969–983.

(15) Knöös, P.; Onder, S.; Pedersen, L.; Piculell, L.; Ulvenlund, S.; Wahlgren, M. Surfactants modify the release from tablets made of hydrophobically modified poly (acrylic acid). *Result Pharm. Sci.* **2013**, *3*, 7–14.

(16) Wang, G.; Wang, J.; Li, F.; To, S. T. Development and evaluation of a novel drug delivery: pluronics/SDS mixed micelle loaded with myricetin in vitro and in vivo. *J. Pharm. Sci.* **2016**, *105*, 1535–1543.

(17) Sharma, G.; Naushad, M.; Thakur, B.; Kumar, A.; Negi, P.; Saini, R.; Chahal, A.; Kumar, A.; Stadler, F. J.; Aqil, U. M. H. Sodium Dodecyl Sulphate-supported nanocomposite as drug carrier system for controlled delivery of ondansetron. *Int. J. Environ. Res.* **2018**, *15*, 414.

(18) Del Sal, G.; Manfioletti, G.; Schneider, C. The CTAB-DNA precipitation method: a common mini-scale preparation of template DNA from phagemids, phages or plasmids suitable for sequencing. *BioTechniques* **1989**, *7*, 514–520.

(19) Nielsen, M. M.; Andersen, K. K.; Westh, P.; Otzen, D. E. Unfolding of beta-sheet proteins in SDS. *Biophys. J.* **2007**, *92*, 3674–3685.

(20) Azmat, M. A.; Khan, I. A.; Cheema, H. M. N.; Rajwana, I. A.; Khan, A. S.; Khan, A. A. Extraction of DNA suitable for PCR applications from mature leaves of Mangifera indica L. *Journal of Zhejiang University. Science. B* **2012**, *13*, 239–243.

(21) Otzen, D. E. Proteins in a brave new surfactant world. *Curr. Opin Colloid In.* **2015**, *20*, 161–169.

(22) Jafari, M.; Mehrnejad, F.; Rahimi, F.; Asghari, S. M. The Molecular Basis of the Sodium Dodecyl Sulfate Effect on Human Ubiquitin Structure: A Molecular Dynamics Simulation Study. *Sci. Rep.* **2018**, *8*, 2150.

(23) Wu, S.-H.; Chen, D.-H. Synthesis of high-concentration Cu nanoparticles in aqueous CTAB solutions. *Journal of Colloid and Interface Science* **2004**, *273*, 165–169.

(24) Sun, X. M.; Chen, X.; Deng, Z. X.; Li, Y. D. A CTAB-assisted hydrothermal orientation growth of ZnO nanorods. *Materials Chemistry and Physics* **2003**, *78*, 99–104.

(25) Smith, D. K.; Korgel, B. A. The Importance of the CTAB Surfactant on the Colloidal Seed-Mediated Synthesis of Gold Nanorods. *Langmuir* **2008**, *24*, 644–649.

(26) Moon, S. Y.; Kusunose, T.; Sekino, T. CTAB-Assisted Synthesis of Size- and Shape-Controlled Gold Nanoparticles in SDS Aqueous Solution. *Materials Letters* **2009**, *63*, 2038–2040.

(27) *Metastable liquids: concepts and principles*; Princeton Univeristy Press, Princeton, NJ, 1996.

(28) Vekilov, P. G. Nucleation. *Crys. Growth Des.* **2010**, *10*, 5007–5019.

(29) Perepezko, J. H. Nucleation in undercooled liquids. *Materials Science and Engineering* **1984**, *65*, 125 – 135, Solidification Microstructure: 30 Years after Constitutional Supercooling.

(30) Greenwood, G. W.; Greer, A. L.; Herlach, D. M.; Kelton, K. F.; Cantor, B. Heterogeneous nucleation and adsorption. *Philosophical Transactions of the Royal Society of London. Series A: Mathematical, Physical and Engineering Sciences* **2003**, *361*, 409–417.

(31) Greenwood, G. W.; Greer, A. L.; Herlach, D. M.; Kelton, K. F.; Perepezko, J. H.; Tong, W. S. Nucleation-catalysis-kinetics analysis under dynamic conditions. *Philosophical Transactions of the Royal Society of London. Series A: Mathematical, Physical and Engineering Sciences* **2003**, *361*, 447–461.

(32) Sear, R. P. Heterogeneous and homogeneous nucleation compared: rapid nucleation on microscopic impurities. *The Journal of Physical Chemistry B* **2006**, *110*, 4985–4989.

(33) Sear, R. P. Nucleation at contact lines where fluid–fluid interfaces meet solid surfaces. *Journal of Physics: Condensed Matter* **2007**, *19*, 466106.

(34) Sear, R. P. Nucleation: theory and applications to protein solutions and colloidal suspensions. *Journal of Physics: Condensed Matter* **2007**, *19*, 033101.

(35) Page, A. J.; Sear, R. P. Heterogeneous nucleation in and out of pores. *Phys. Rev. Lett.* **2006**, *97*, 065701.

(36) Frenkel, D. Seeds of phase change. *Nature* **2006**, *443*, 641–641.

(37) Diao, Y.; Myerson, A. S.; Hatton, T. A.; Trout, B. L. Surface Design for Controlled Crystallization: The Role of Surface Chemistry and Nanoscale Pores in Heterogeneous Nucleation. *Langmuir* **2011**, *27*, 5324–5334.

(38) Carter, P. W.; Ward, M. D. Directing polymorph selectivity during nucleation of anthranilic acid on molecular substrates. *Journal of the American Chemical Society* **1994**, *116*, 769–770.

(39) D'Souza, S. M.; Alexander, C.; Carr, S. W.; Waller, A. M.; Whitcombe, M. J.; Vulfson, E. N. Directed nucleation of calcite at a crystal-imprinted polymer surface. *Nature* **1999**, *398*, 312–316.

(40) Lee, A. Y.; Lee, I. S.; Dette, S. S.; Boerner, J.; Myerson, A. S. Crystallization on Confined Engineered Surfaces: A Method to Control Crystal Size and Generate Different Polymorphs. *Journal of the American Chemical Society* **2005**, *127*, 14982–14983.

(41) Lee, T.; Hung, S. T.; Kuo, C. S. Polymorph farming of acetaminophen and sulfathiazole on a chip. *Pharm Res* **2006**, *23*, 2542–2555.

(42) Wang, H.; Khodaparast, S.; Carroll, J.; Kelly, C.; Robles, E. S. J.; Cabral, J. T. A microfluidic-multiwell platform for rapid phase mapping of surfactant solutions. *Review of Scientific Instruments* **2020**, *91*, 045109.

(43) Adamo, M.; Poulos, A. S.; G. Lopez, C.; Martel, A.; Porcar, L.; Cabral, J. T. Droplet microfluidic SANS. *Soft Matter* **2018**, *14*, 1759–1770.

(44) Summerton, E.; Zimbitas, G.; Britton, M.; Bakalis, S. Crystallisation of sodium dodecyl sulfate and the corresponding effect of 1-dodecanol addition. *Journal of Crystal Growth* **2016**, *455*, 111–116.

(45) Smith, L. A.; Hammond, R. B.; Roberts, K. J.; Machin, D.; McLeod, G. Determination of the crystal structure of anhydrous sodium dodecyl sulphate using a combination of synchrotron radiation powder diffraction and molecular modelling techniques. *J. Molec. Struct.* **2000**, *554*, 173 –182.

(46) Smith, L.; Duncan, A.; Thomson, G.; Roberts, K.; Machin, D.; McLeod, G. Crystallisation of sodium dodecyl sulphate from aqueous solution: phase identification, crystal morphology, surface chemistry and kinetic interface roughening. *Journal of Crystal Growth* **2004**, *263*, 480–490.

(47) Miller, R. M.; Poulos, A. S.; Robles, E. S. J.; Brooks, N. J.; Ces, O.; Cabral, J. T. Isothermal Crystallization Kinetics of Sodium Dodecyl Sulfate–Water Micellar Solutions. *Crystal Growth & Design* **2016**, *16*, 3379–3388.

(48) Miller, R. M.; Ces, O.; Brooks, N. J.; Robles, E. S. J.; Cabral, J. T. Crystallization of Sodium Dodecyl Sulfate-Water Micellar Solutions under Linear Cooling. *Cryst. Growth Des.* **2017**, *17*, 2428–2437.

(49) Lioliou, M. G.; Paraskeva, C. A.; Koutsoukos, P. G.; Payatakes, A. C. Heterogeneous nucleation and growth of calcium carbonate on calcite and quartz. *Journal of Colloid and Interface Science* **2007**, *308*, 421 –428.

(50) Chatterjee, A. M.; Price, F. P.; Newman, S. Heterogeneous nucleation of crystallization of high polymers from the melt. I. Substrate-induced morphologies. *Journal of Polymer Science: Polymer Physics Edition* **1975**, *13*, 2369–2383.

(51) Schonhorn, H. Heterogeneous Nucleation of Polymer Melts on High-Energy Surfaces. II. Effect of Substrate on Morphology and Wettability. *Macromolecules* **1968**, *1*, 145–151.

(52) Chayen, N. E.; Saridakis, E.; Sear, R. P. Experiment and theory for heterogeneous nucleation of protein crystals in a porous medium. *Proceedings of the National Academy of Sciences* **2006**, *103*, 597–601.

(53) Diao, Y.; Harada, T.; Myerson, A. S.; Hatton, T. A.; Trout, B. L. The role of nanopore shape in surface-induced crystallization. *Nat Mater* **2011**, *10*, 867–871.

(54) Arnold, O. et al. Mantid—Data analysis and visualization package for neutron scattering and μSR experiments. *Nucl. Instrum. Meth. A* **2014**, *764*, 156–166.

(55) Rasel, M. S. U.; Park, J.-Y. A sandpaper assisted micro-structured polydimethylsiloxane fabrication for human skin based triboelectric energy harvesting application. *Applied Energy* **2017**, *206*, 150 – 158.

(56) Leigh, I. D.; McDonald, M. P.; Wood, R. M.; Tiddy, G. J. T.; Trevethan, M. A. Structure of liquid-crystalline phases formed by sodium dodecyl sulphate and water as determined by optical microscopy, X-ray diffraction and nuclear magnetic resonance spectroscopy. *J. Chem. Soc., Faraday Trans. 1* **1981**, *77*, 2867–2876.

(57) Kekicheff, P.; Grabielle, M. C.; Ollivon, M. Phase diagram of sodium dodecyl sulfate-water system: 1. A calorimetric study. *J. Colloid Interf. Sci.* **1989**, *131*, 112 – 132.

(58) Itri, R.; Amaral, L. Q.; Mariani, P. Structure of the hexagonal phase of the sodium dodecyl sulfate and water system. *Phys. Rev. E* **1996**, *54*, 5211–5216.

(59) Lee, T.; Yeh, K. L.; You, J. X.; Fan, Y. C.; Cheng, Y. S.; Pratama, D. E. Reproducible Crystallization of Sodium Dodecyl Sulfate·1/8 Hydrate by Evaporation, Antisolvent Addition, and Cooling. *ACS Omega* **2020**, *5*, 1068–1079.

(60) Moroi, Y.; Motomura, K.; Matuura, R. The critical micelle concentration of sodium dodecyl sulfate-bivalent metal dodecyl sulfate mixtures in aqueous solutions. *Journal of Colloid and Interface Science* **1974**, *46*, 111–117.

(61) Hammouda, B. Temperature effect on the nanostructure of SDS micelles in water. *J. Res. Natl. Inst. Stan.* **2013**, *118*, 151–167.

(62) Khodaparast, S.; Sharratt, W. N.; Tyagi, G.; Dalgliesh, R. M.; Robles, E. S.; Cabral, J. T. Pure and mixed aqueous micellar solutions of Sodium Dodecyl sulfate

(SDS) and Dimethyldodecyl Amine Oxide (DDAO): Role of temperature and composition. *Journal of Colloid and Interface Science* **2021**, *582*, 1116 – 1127.

(63) Kadam, S. S.; Kulkarni, S. A.; Ribera, R. C.; Stankiewicz, A. I.; ter Horst, J. H.; Kramer, H. J. M. A new view on the metastable zone width during cooling crystallization. *Chem. Eng. Sci.* **2012**, *72*, 10–19.

(64) van Gelder, R.; Roberts, K.; Chambers, J.; Instone, T. Nucleation of single and mixed straight chain surfactants from dilute aqueous solutions. *Journal of Crystal Growth* **1996**, *166*, 189 – 194.

(65) Söhnel, O.; Mullin, J. W. Interpretation of crystallization induction periods. *Journal of Colloid and Interface Science* **1988**, *123*, 43–50.

(66) Cardew, P. T.; Davey, R. J.; Garside, J. Evaluation of supersaturation in crystal growth from solution. *Journal of Crystal Growth* **1979**, *46*, 534–538.

(67) Artusio, F.; Pisano, R. Surface-induced crystallization of pharmaceuticals and biopharmaceuticals: A review. *Int J Pharm* **2018**, *547*, 190–208.

(68) Archer, A. J.; Malijevský, A. Crystallization of soft matter under confinement at interfaces and in wedges. *Journal of Physics: Condensed Matter* **2016**, *28*, 244017.

(69) Grossier, R.; Magnaldo, A.; Veesler, S. Ultra-fast crystallization due to confinement. *Journal of Crystal Growth* **2010**, *312*, 487 – 489.

(70) Kirby, B. J.; Hasselbrink Jr., E. F. Zeta potential of microfluidic substrates: 2. Data for polymers. *ELECTROPHORESIS* **2004**, *25*, 203–213.

(71) Naseh, N.; Mohseni, M.; Ramezanzadeh, B. Role of surface active additives on reduction of surface free energy and enhancing the mechanical Attributes of easy-to-clean automotive clearcoats: Investigating resistance against simulated tree gum. *Int. J. Adhes. Adhes.* **2013**, *44*, 209–219.

(72) Zhang, R.; Somasundaran, P. Advances in adsorption of surfactants and their mixtures at solid/solution interfaces. *Adv. Colloid Interface Sci.* **2006**, *123-126*, 213–229.

(73) McKechnie, D.; Anker, S.; Zahid, S.; Mulheran, P. A.; Sefcik, J.; Johnston, K. Interfacial Concentration Effect Facilitates Heterogeneous Nucleation from Solution. *The Journal of Physical Chemistry Letters* **2020**, *11*, 2263–2271.

(74) Vitha, M. F.; Carr, P. W. Study of the Polarity and Hydrogen-Bond Ability of Dodecyltrimethylammonium Bromide Micelles by the KamletTaft Solvatochromic Comparison Method. *J. Phys. Chem. B* **1998**, *102*, 1888–1895.

(75) Abenojar, J.; Martínez, M.; Encinas, N.; Velasco, F. Modification of glass surfaces adhesion properties by atmospheric pressure plasma torch. *International Journal of Adhesion and Adhesives* **2013**, *44*, 1–8.

(76) Terpilowski, K.; Rymuszka, D. Surface properties of glass plates activated by air, oxygen, nitrogen and argon plasma. *Glass Physics and Chemistry* **2016**, *42*, 535–541.

(77) Rymuszka, D.; Terpiłowski, K.; Hołysz, L. Influence of Volume Drop on Surface Free Energy of Glass. *Annales UMCS, Chemia* **2014**, *68*, 121–132.

(78) Kim, Y. G.; Lim, N.; Kim, J.; Kim, C.; Lee, J.; Kwon, K.-H. Study on the surface energy characteristics of polydimethylsiloxane (PDMS) films modified by C4F8/O2/Ar plasma treatment. *Applied Surface Science* **2019**, *477*, 198–203.

(79) Vicente, C.; André, P.; Ferreira, R. Simple measurement of surface free energy using a web cam. *Revista Brasileira de Ensino de Física* **2012**, *34*, 1–5.

(80) Chibowski, E.; Terpilowski, K. Surface free energy of polypropylene and polycarbonate solidifying at different solid surfaces. *Applied Surface Science* **2009**, *256*, 1573–1581.

(81) Surface tension values of some common test liquids for surface energy analysis. `http://www.surface-tension.de/solid-surface-energy.htm`.

(82) Owens, D. K.; Wendt, R. C. Estimation of the surface free energy of polymers. *Journal of Applied Polymer Science* **1969**, *13*, 1741–1747.

(83) Sirringhaus, H.; Brown, P. J.; Friend, R. H.; Nielsen, M. M.; Bechgaard, K.; Langeveld-Voss, B. M. W.; Spiering, A. J. H.; Janssen, R. A. J.; Meijer, E. W.; Herwig, P.; de Leeuw, D. M. Two-dimensional charge transport in self-organized, high-mobility conjugated polymers. *Nature* **1999**, *401*, 685–688.

(84) Afzali, A.; Dimitrakopoulos, C. D.; Breen, T. L. High-Performance, Solution-Processed Organic Thin Film Transistors from a Novel Pentacene Precursor. *Journal of the American Chemical Society* **2002**, *124*, 8812–8813.

(85) Kim, N.; Kee, S.; Lee, S. H.; Lee, B. H.; Kahng, Y. H.; Jo, Y.-R.; Kim, B.-J.; Lee, K. Highly Conductive PEDOT:PSS Nanofibrils Induced by Solution-Processed Crystallization. *Advanced Materials* **2014**, *26*, 2268–2272.

(86) Schniepp, H. C.; Shum, H. C.; Saville, D. A.; Aksay, I. A. Orientational Order of Molecular Assemblies on Rough Surfaces. *The Journal of Physical Chemistry C* **2008**, *112*, 14902–14906.

(87) Ma, X.; Zhang, S.; Jiao, F.; Newcomb, C. J.; Zhang, Y.; Prakash, A.; Liao, Z.; Baer, M. D.; Mundy, C. J.; Pfaendtner, J.; Noy, A.; Chen, C.-L.; De Yoreo, J. J. Tuning crystallization pathways through sequence engineering of biomimetic polymers. *Nature Materials* **2017**, *16*, 767–774.

(88) Striolo, A.; Grady, B. P. Surfactant Assemblies on Selected Nanostructured Surfaces: Evidence, Driving Forces, and Applications. *Langmuir* **2017**, *33*, 8099–8113.

(89) Yan, D.; Zeng, Q.; Xu, S.; Zhang, Q.; Wang, J. Heterogeneous Nucleation on Concave Rough Surfaces: Thermodynamic Analysis and Implications for Nucleation Design. *The Journal of Physical Chemistry C* **2016**, *120*, 10368–10380.

(90) Campbell, J. M. On topography and crysatl nucleation. Ph.D. thesis, Univeristy of Leeds, 2014.

(91) Sholl, C.; Fletcher, N. Decoration criteria for surface steps. *Acta Metallurgica* **1970**, *18*, 1083–1086.

(92) Page, A. J.; Sear, R. P. Crystallization Controlled by the Geometry of a Surface. *Journal of the American Chemical Society* **2009**, *131*, 17550–17551.

(93) Bi, Y.; Cao, B.; Li, T. Enhanced heterogeneous ice nucleation by special surface geometry. *Nature Communications* **2017**, *8*, 15372.

(94) Walker, C.; Lerch, S.; Reininger, M.; Eghlidi, H.; Milionis, A.; Schutzius, T. M.; Poulikakos, D. Desublimation Frosting on Nanoengineered Surfaces. *ACS Nano* **2018**, *12*, 8288–8296.

(95) Zeng, Q.; Xu, S. Thermodynamics and Characteristics of Heterogeneous Nucleation on Fractal Surfaces. *The Journal of Physical Chemistry C* **2015**, *119*, 27426–27433.

(96) Holbrough, J. L.; Campbell, J. M.; Meldrum, F. C.; Christenson, H. K. Topographical Control of Crystal Nucleation. *Crystal Growth & Design* **2012**, *12*, 750–755.

(97) Zhang, Y.; Wang, M.; Lin, X.; Huang, W. Effect of Substrate Surface Microstructure on Heterogeneous Nucleation Behavior. *Journal of Materials Science Technology* **2012**, *28*, 67–72.

(98) ISIS Neutron and Muon Source experiments RB1820374. `https://doi.org/10.5286/ISIS.E.RB1820374`.

Graphical TOC Entry